Pedestal Stability Comparison and ITER Pedestal Prediction

P.B. Snyder 1), N. Aiba 2), M. Beurskens 3), R.J. Groebner 1), L.D. Horton 4), A.E. Hubbard 5),
J.W. Hughes 5), G.T.A. Huysmans 6), Y. Kamada 2), A. Kirk 3), C. Konz 4), A.W. Leonard 1),
J. Lönnroth 3), C.F. Maggi 4), R. Maingi 7), T.H. Osborne 1), N. Oyama 2), A. Pankin 8),
S. Saarelma 3), G. Saibene 9), J.L. Terry 5), H. Urano 2), and H.R. Wilson 10)

1) General Atomics, PO Box 85608, San Diego, California 92186-5608, USA
2) Fusion Research and Development Directorate, JAEA, Naka, Ibaraki, Japan
3) EURATOM/UKAEA Fusion Association, Culham Science Centre, Abingdon, UK
4) MPI für Plasmaphysik, EURATOM Association, Garching, Germany
5) MIT Plasma Science and Fusion Center, Cambridge, Massachusetts, USA
6) Association Euratom/CEA, Cadarache, St Paul-lez-Durance, France
7) Oak Ridge National Laboratory, Oak Ridge, Tennessee, USA
8) Lehigh University, Bethlehem, Pennsylvania, USA
9) EFDA Close Support Unit-Garching, Garching, Germany
10) University of York, York, UK

e-mail contact of main author: snyder@fusion.gat.com

Abstract. The pressure at the top of the edge transport barrier (or "pedestal height") strongly impacts fusion performance, while large edge localized modes (ELMs), driven by the free energy in the pedestal region, can constrain material lifetimes. Accurately predicting the pedestal height and ELM behavior in ITER is an essential element of prediction and optimization of fusion performance. Investigation of intermediate wavelength MHD modes (or "peeling-ballooning" modes) has led to improved understanding of important constraints on the pedestal height and the mechanism for ELMs. The combination of high resolution pedestal diagnostics, including substantial recent improvements, and a suite of highly efficient stability codes, has made edge stability analysis routine on several major tokamaks, contributing both to understanding, and to experimental planning and performance optimization. Here we present extensive comparisons of observations to predicted edge stability boundaries on several tokamaks, both for the standard (Type I) ELM regime, and for small ELM and ELM-free regimes. We further use the stability constraint on pedestal height to test models of the pedestal width, and self-consistently combine a simple width model with peeling-ballooning stability calculations to develop a new predictive model (EPED1) for the pedestal height and width. This model is tested against experimental measurements, and used in initial predictions of the pedestal height for ITER.

1. Introduction

Accurate prediction of both the pedestal height [pressure at the inside of the shaded region in Fig. 1(a)] and edge localized mode (ELM) behavior is essential for prediction and optimization of ITER performance. Pedestal stability studies have developed into a useful and standard tool for understanding both pedestal and ELM characteristics in tokamaks. Here we discuss the basics of peeling-ballooning theory and numerics (Sec. 2), calculations of edge stability in experiment and their implications (Sec. 3), and pedestal width physics (Sec. 4). Finally, we combine stability calculations and a simple pedestal width model to develop a predictive model of the pedestal height and width (EPED1), test it against experiment, and present initial predictions for the ITER pedestal height (Sec. 5).

2. Peeling-ballooning Theory and Code Development

The peeling-ballooning model of ELMs posits that free energy from the strong pressure gradient and resulting large bootstrap current [Fig. 1(a)] in the edge barrier, or "pedestal," region drive intermediate wavelength (typically $n\sim3$–30) modes which constrain the pedestal height and trigger ELMs. A schematic diagram of peeling-ballooning stability boundaries is given in Fig. 1(b), and a typical 3D structure of such a mode is shown in Fig. 1(c) [1]. As shown in Fig. 1(b), the stability boundary varies strongly with plasma shape, and the trajectory with which the pedestal evolves toward its stability limit is strongly impacted by collisionality (ν^*). At high ν^*, the bootstrap current is suppressed and relatively high $n\sim10$–30 ballooning

modes are limiting, while at low $\nu*$, relatively low $n\sim3$–6 current-driven kink/peeling modes are limiting. Many high performance H-mode discharges operate at moderate $\nu*$, where the pedestal height and overall performance are maximized, and intermediate $n\sim5$–20 peeling-ballooning modes provide the constraint on the pedestal height.
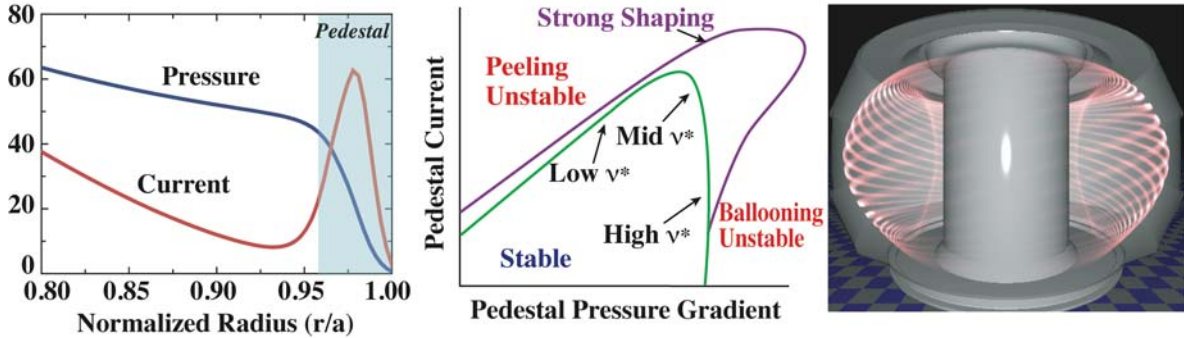

FIG. 1. (a) Typical profiles in the edge barrier or "pedestal" (shaded) region. (b) Schematic diagram of pedestal stability, including impact of shaping and collisionality. (c) Typical peeling-ballooning mode structure in 3D (n=19).

The hypothesis that ELMs are driven by MHD modes has existed essentially since the discovery of H-mode. The importance of peeling-ballooning coupling was noted in high-n studies [2]. Extension of the theory to higher order, and its numerical implementation in the ELITE code, allowed quantitative treatment of intermediate-n modes, and successful comparisons to experiment [3,4]. In parallel, a number of efficient MHD codes, including MISHKA [5,6], MARG2D [7,8], KINX [9], ILSA [10], DCON and GATO [11], were employed for the study of intermediate-n edge stability in tokamaks. A pair of recent reviews [6,12] summarize many results. The availability of multiple codes employing a variety of numerical methods has allowed extensive code verification [e.g. 3,4,8,13]. An example is given in Fig. 2(a). Here GATO (n=1–19), MARG2D (n=5–160), and ELITE (n=4–1000) find good quantitative agreement in growth rate for a D-shaped equilibrium with pedestal profiles, but no X-point. The ELITE results for n=800–1000 are used to extrapolate the n=∞ growth rate, showing good agreement with BAL-MSC. This result also shows that infinite-n theory, while quite useful for insight, cannot be used quantitatively in the pedestal, as it is generally only valid for n's higher than the diamagnetic ($n\sim25$–60) or FLR ($n\sim40$–300) cutoff.
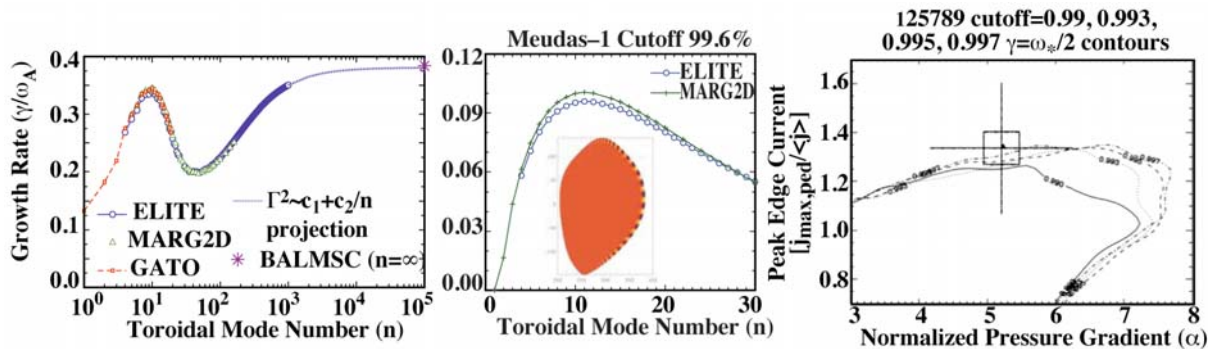

FIG. 2. Benchmark of MHD codes in (a) limiter and (b) near X-point geometry, with n=11 mode structure inset. (c) Effect of cutoff on stability bound for a QH mode discharge, showing impact of cutoff is small provided cutoff is sufficiently far out (here $>\sim99.3\%$).

Obtaining precise growth rates for experimental equilibria, which often contain X-points, can be more challenging. Relatively high RZ grid resolution is required for high precision, particularly in the vicinity of the X-point. Figure 2(b) shows a comparison of MARG2D and ELITE for a JT-60U-like equilibrium cut off at the 99.6% flux surface. Good agreement is

obtained here, and at a 99.8% cutoff, via use of a very high resolution (1025x1025) equilibrium. ILSA finds somewhat lower growth rates for this case [10]. Fortunately, for experimental comparisons, such very high precision is generally not needed. One need only determine the stability boundary [Fig. 1(b) or 3(a–c)] to substantially better accuracy than the measurement error bars for the pressure gradient (typically ~10%–25%), which can typically be achieved at resolutions ~129x129. Similarly, while the effect of the approach to the X-point is a subject of significant theoretical and numerical interest [6,9,10,15], for realistic experimental profiles, the impact of cutoff changes on the stability boundary is found, in the several cases studied, to be small compared to measurement uncertainty, provided the cutoff is sufficiently far out to retain the sharp gradient region. Typically $\psi > ~99.4\%$ is sufficient, as shown in Fig. 2(c). Most results discussed here use a cutoff in the range 99.5%–99.7%.

3. Pedestal Stability Calculation in Experiment and its Implications

The implementation of high resolution diagnostic systems has allowed accurate measurement of profiles in the edge barrier region necessary for rigorous testing of the peeling-ballooning model of ELMs. Such tests, involving high resolution equilibrium reconstruction and MHD stability calculation over a wide range of mode numbers (typically $n\sim3$–30), have now been successfully conducted on all of the world's major tokamaks in well over 100 different discharges [1,4,6,9,11–14,16–23,25,28,34]. Numerous comparison experiments between machines, as well as dedicated experiments on particular devices, have elucidated the role of shape [4,8,9,18,20], aspect ratio [14,18,19], beta [13,20], collisionality [4,12], and rotation [13,14,19,22] on edge stability.

A direct method to study experimental pedestal stability is to construct a time series of equilibria, or a single equilibrium near the maximum observed pedestal height (shortly before an ELM), and then perturb the values of pressure gradient and current around the observed reference point, calculating $n\sim3$–30 stability at each point to construct a stability boundary, as in Figs. 3(a–c). These pedestal stability diagrams are typically cast in terms of two local parameters, such as the maximum normalized pressure gradient (α) in the edge barrier, and a characteristic parallel current [Figs. 1(b) and 3(a,c)] or magnetic shear [Fig. 3(b)] in the pedestal. It is important to keep in mind, however, that pedestal stability is not local. In general the shape of the profiles throughout the pedestal region and into the core impacts pedestal stability. Because a broadened pedestal increases overall drive for broader modes, the maximum stable gradient is not a constant but rather decreases with pedestal width, roughly $p_{ped}\sim\Delta^{3/4}$, where Δ is the pedestal width in normalized poloidal flux (Ψ_N).
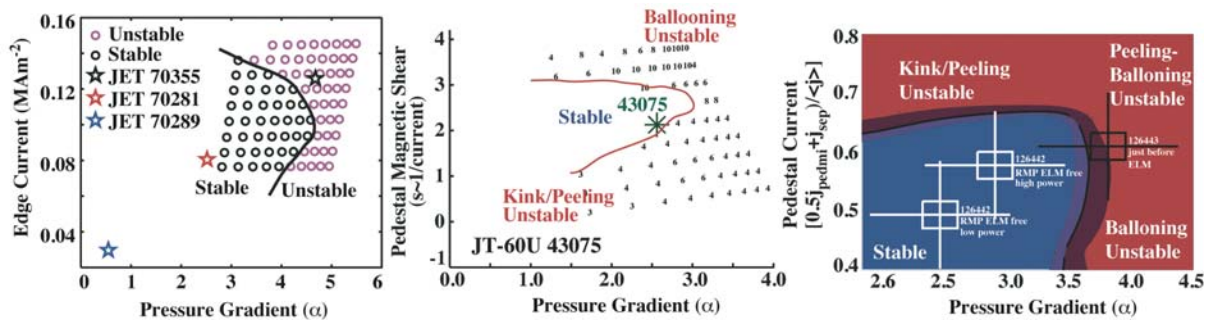

FIG. 3. Pedestal stability diagrams for experiments on (a) JET (b) JT-60U and (c) DIII-D, showing Type I ELMs occurring near stability bound (JET 70355, JT-60U 43075, DIII-D 126443), while other types of discharges (radiative Type III JET 70281 and 70289, and RMP ELM-free DIII-D 126442) can lie in the stable region.

For standard Type I ELMing discharges, such as JET 70355 in Fig. 3(a) [16,17], JT-60U 43075 [19,22] in Fig. 3(b), and DIII-D 126443 in Fig. 3(c), it is consistently found that the pedestal approaches the stability boundary and crosses it at approximately the time an ELM is observed (at which time the pedestal height is reduced, and the cycle repeats). We define a

relative distance to the stability boundary D as the ratio of the distance from the origin of a j–α diagram [e.g. Fig. 3(c)] to the operational point, over the distance to the stability bound along a line passing through the operational point. For 39 recent DIII-D Type I ELM discharges, for which stability has been studied shortly before an ELM, we find a ratio D=1.05±0.19, consistent with the conclusion that peeling-ballooning stability constrains the pedestal and triggers observed ELMs.

Because of the potential impact of large ELMs on plasma facing materials on ITER, a number of techniques have been developed to avoid or mitigate large Type I ELMs. These include both passive (e.g. Quiescent H-Mode, Type II, Type III, Grassy ELMs, EDA) and active (e.g. RMP, pellets, impurity injection) ELM control techniques. Stability studies on these discharges provide important insight into the mechanisms for ELM mitigation.

The use of imposed resonant magnetic perturbations (RMP) to suppress ELMs has been demonstrated on DIII-D [25], and is planned for ITER. Edge stability studies on ELM suppressed discharges (using 2D equilibria) have consistently found them to lie in the stable region. A typical example is shown in Fig. 3(c) (white crosshairs). Both the low and high power phases of discharge 126442, where ELMs are suppressed with 6.3 kA of current in n=3 coils, lie well inside the stable region. An otherwise identical discharge with zero RMP current, 126443 (black crosshair), evolves to the stability limit and exhibits Type I ELMs. Stability analysis of 15 DIII-D RMP ELM-free timeslices finds a stability ratio D=0.83±0.10, consistent with operation significantly below the stability boundary. Hence no effect of the RMP perturbation on stability itself is required to explain ELM suppression. Rather, enhanced particle transport associated with the RMP appears to hold edge gradients below the stability limit. Recently, ELMs have been mitigated, but not fully suppressed, via n=1 perturbations from the error correction coils on JET [26]. Analysis of these discharges finds a reduction in pedestal density, but pedestal temperature is sufficiently high that the pedestal is near the low-n kink/peeling stability boundary [17]. It is suggested that these current-driven modes are responsible for the remaining small ELMs in these discharges.

In a recent set of advanced tokamak JET experiments [16], it was found that increasing the radiation fraction by either impurity injection or deuterium gas puffing can significantly reduce ELM size. Stability analysis [16,17], taking advantage of high resolution profile measurements from a new Thomson scattering system, finds that for low radiation fractions where Type I ELMs occur, the stability boundary is reached as expected before an ELM [Fig. 3(a)]. However, at higher radiative fraction the pedestal height is reduced and the ELMs become Type III. The stability analysis finds these highly radiative discharges 70281 and 70289 to be stable. More generally, it has been consistently found that high density Type III ELM discharges lie below the ideal stability boundary, and these small ELMs are presumably driven by resistive or kinetic instabilities. Similarly, on Alcator C-Mod, ELM-free EDA mode operation is found to occur below the stability boundary, while the appearance of small or large ELMs is associated with crossing the stability bound [23].

It has long been suggested [2,4] that higher-n ballooning modes [Fig. 1(b)], which are relatively narrow and do not need to dissipate current to stabilize themselves, should trigger relatively small ELMs. This is consistent with the widely observed decrease in ELM size at high collisionality [27]. Both the onset of small Type I ELMs in DIII-D [4] and grassy ELMs in JT-60U, which occur at *low* collisionality [21], have been associated with relatively narrow modes. A recent study of Type II ELM discharges on JET [17], finds that the combination of deep second stability access near double null, and relatively high collisionality, causes the discharges to be limited by relatively high-n modes with narrow mode structures.

Quiescent H-Mode (QH) discharges, with no ELMs and a relatively steady, rotating low-n mode in the edge, were first discovered at very low density with neutral beam injection in the counter-current direction. Stability analysis [Fig. 2(c)], finds that QH modes operate near the low-n kink/peeling stability boundary in the edge [13,28]. By optimizing discharge shape to increase the density at which the transition from kink/peeling limited to peeling-ballooning limited occurs, more than a doubling of allowed density in QH mode discharges was

achieved [13], up to Greenwald fractions of 0.6. Furthermore, it was suggested that strong rotation shear facilitates the saturation of the low-n kink/peeling mode, resulting in the edge harmonic oscillation (EHO), and it was predicted that co-rotating QH modes should be possible if sufficient flow shear could be achieved. In 2008, co-rotating QH mode discharges with very strong edge rotation shear were produced on DIII-D [28]. This stability model allows prediction of required pedestal density for QH operation in ITER, but further work is needed to fully quantify requirements on rotation shear.

While stability studies have elucidated several aspects of operation in small and no-ELM regimes, a number of important, ITER-relevant issues remain unresolved. These include quantitative understanding of transport, sources and sinks in RMP discharges, quantitative predictions of ELM size, quantification of the conditions for robust EHO saturation and successful QH-mode operation, requirements for and characterization of pellet-induced ELMs, and theoretical understanding of conditions for operation in Type III and EDA regimes.

4. Pedestal Width Observations and Models

Pedestal stability calculations provide a constraint on the pedestal height as a function of pedestal width. Studies have demonstrated that it is possible to predict these stability boundaries with reasonable accuracy by using model equilibria characterized by a relatively small set of parameters [18]. These calculations can be used to predict the pedestal height, provided the pedestal width is known beforehand.

A number of models have been developed and experiments performed to study physics of the pedestal width [Ref. 29 and references therein]. However, until recently, results have been ambiguous, due in part to two key issues: 1) the narrow pedestal width is difficult to measure accurately, and small changes in the width are particularly difficult to assess, and 2) stability physics imposes a strong and complex constraint on the pedestal width, schematically $p_{ped} \sim \Delta^{3/4} S$, where S has a complex dependence on shape, collisionality, current, field etc. This constraint implies that the width will correlate strongly with most parameters related to pedestal height, and that complex dependencies on density and temperature can be due to the stability constraint (via collisional effects on bootstrap current), rather than the physics inherent to the width itself.
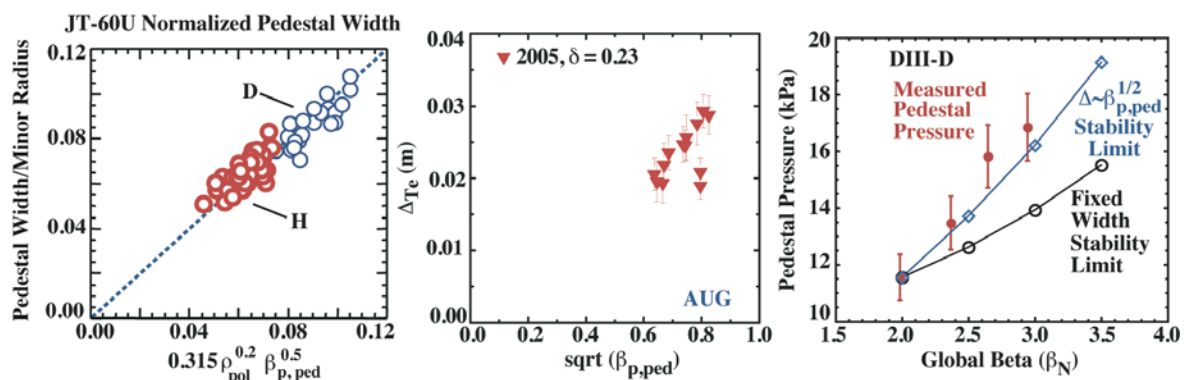

FIG. 4. (a) JT-60U experiment with multiple mass species finds $\beta_{p,ped}^{1/2}$ width scaling with weak dependence on mass. (b) AUG experiment finds similar scaling in T_e (but not n_e) pedestal width. (c) Taking into account both a $\beta_{p,ped}^{1/2}$ width scaling and the Shafranov shift effect on pedestal stability can explain observations in beta-scan experiments on DIII-D.

Three important recent methods have been used to clarify pedestal width physics: 1) carefully designed experiments using high resolution edge diagnostics, 2) accounting for the stability constraint when analyzing results of width experiments, and 3) combining pedestal width models with full calculations of edge stability to yield predictive models which can be tested directly against pedestal height, which can be measured more accurately (Sec. 5).

Early studies [e.g. 30] found pedestal width correlations with pedestal beta poloidal ($\beta_{p,ped}$) and with poloidal and toroidal gyroradius ($\rho_{\theta i}, \rho_i$). An experiment on JT-60U used a variation in species mass (H and D) to separate these scalings [31]. No appreciable difference in pedestal width for similar discharges in H and D was found, implying weak or no ρ_i or $\rho_{\theta i}$ dependence. Results appear consistent with a $\beta_{p,ped}^{1/2}$ scaling, as shown in Fig. 4(a) [31]. Recent hydrogen experiments on DIII-D appear to confirm this result [32]. Similarly, dimensionless scans on JET and DIII-D find weak or no dependence on ρ/a. Measurements of T_e width on AUG also appear consistent with a $\beta_{p,ped}^{1/2}$ scaling [Fig. 4(b)], though weak or no dependence is seen in the density width [24].

A comparison experiment between AUG and DIII-D investigated global β (or power) dependence of the pedestal [20,24]. Investigation of the pedestal height increase with global β [20] found that much of the effect could be explained by the expected impact of Shafranov shift on edge stability [13]. But this effect alone, at constant pedestal width, was not sufficient to explain observed pedestal height, as shown in Fig. 4(c). However, combining a pedestal width which increases with $\beta_{p,ped}^{1/2}$ with the stability calculations, it is possible to explain the observations in both beta and shape scaling experiments [Fig. 4(c)] [20]. Similarly, examination of the DIII-D pedestal database has found a good fit to a $\beta_{p,ped}^{1/2}$ width scaling, and notably, once this $\beta_{p,ped}^{1/2}$ dependence is taken into account, dependence of the DIII-D pedestal width on other dimensionless parameters (q, ρ_i, $\rho_{\theta i}$, ν^*, β) is weak [33].

5. Tests of a Predictive Pedestal Model and Predictions for ITER

Combining insight from theory and observation, we propose a predictive model of the pedestal height (EPED1). The EPED1 model consists of two hypotheses which together allow a well-defined predictive model: A) That the pedestal height in high performance H-modes is constrained by intermediate-n edge stability, which can be characterized via a series of 2D model equilibria and a $\gamma > \omega_{*pi}/2$ criterion, and B) the pedestal width can be characterized as $\Delta = c_1 \beta_{p,ped}^{1/2}$, where Δ is the average of the n_e and T_e widths in normalized poloidal flux (Ψ_N), and $c_1 = 0.076$ [33].

The EPED1 model employs stability calculations with ELITE (n=5–30) on series of full 2D model equilibria (as in Refs. 18,33), in which the pedestal temperature is raised until the stability boundary is found. By keeping the pedestal width consistent with $\Delta = 0.076 \beta_{p,ped}^{1/2}$ we locate the point satisfying both hypotheses (A) and (B). Essentially, the stability calculations give the predicted height as a function of predicted width, and the width model gives the predicted width as a function of predicted height. Because the width dependence of the stability constraint (roughly $p_{ped} \sim \Delta^{3/4}$) and the width model ($p_{ped} \sim \Delta^2$) are quite different, there is generally a single non-trivial point in the (p_{ped}, Δ) parameter space where the two constraints intersect: this is the EPED1 height and width prediction. The inputs to the model are a set of operational parameters (B_T, I_p, R, a, κ, δ) and a pair of plasma physics parameters (global β, $n_{e,ped}$), and the outputs are pedestal height and width. Note that if any of the inputs are not known precisely beforehand, predictions can be made for a range of input values.

This model can be rigorously tested against observations of both pedestal height and width across multiple devices, and used to make predictions for future experiments and devices. Note that hypotheses (A) and (B) are strongly coupled in the model. If either the stability constraint or the width model is incorrect, both the predicted height and width should be systematically incorrect. For example, if the constant $c_1 = 0.076$ is too high (low), both height and width predictions would be systematically high (low). If there is a missing dependence in the width model (eg on q, ρ_i, $\rho_{\theta i}$, ν^*, β, a/R), then the accuracy of EPED1 predictions would vary as a function of that parameter.

EPED1 has been successfully tested on systematic parameter scans on DIII-D, and against a random selection of 20 discharges from the DIII-D pedestal database [33]. A dedicated DIII-D experiment was planned to test the model against optimized pedestal measurements, with a very large variation in the pedestal parameters produced via triangularity (δ), I_p at fixed B_T, and I_p at fixed I_p/B_T variations of a factor of ~3 [32]. EPED1

predictions, presented before the experiment, agree well with observations, and produce the correct trends in each individual scan. Using the input values achieved in the experiment, predicted/measured ratios of 1.03±0.13 in height and 0.93±0.15 in width are found over 17 discharges in which pedestal height varied a factor of 10 and width a factor of 3, as shown by blue circles in Fig. 5(a,b). EPED1 has also been employed in an initial prediction for JET AT discharge 70355. Given parameters from Ref. [16], EPED1 predicts a pedestal temperature of 1.45 keV, in reasonable agreement with the observed value of ~1.3 keV, tentatively suggesting the lack of size dependence in the width model (B) is correct.
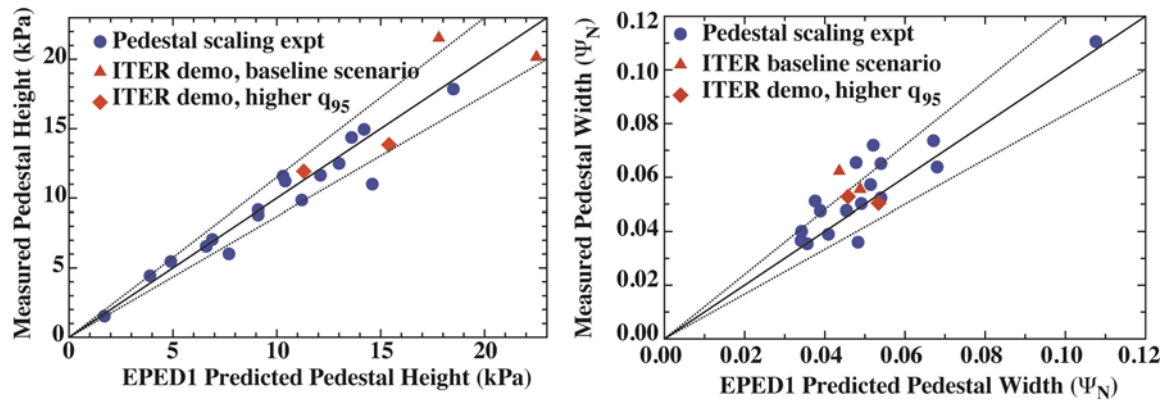

FIG. 5. Test of EPED1 model predictions of (a) pedestal height and (b) width, in a dedicated DIII-D experiment (blue circles). Results also shown for two ITER demonstration baseline scenario discharges (red triangles) and two ITER shape higher q_{95} discharges (red diamonds).

A series of ITER demonstration experiments has been conducted, in which DIII-D is used as a 1/3.7 scale model of ITER [34]. These provide a useful test of EPED1 and its ability to make accurate predictions for ITER. EPED1 predictions are compared to observations for 2 baseline (Scenario 2, q_{95}~3.1) discharges and 2 reduced current (q_{95}~4.5) discharges in Figs. 5(a,b). The ratio of predicted/observed height in these 4 cases is 1.00±0.14. Overall, for the 41 DIII-D discharges studied thus far, the ratio of predicted to observed height is 1.00±0.18 and width 0.96±0.19. A wide range in q, ν^*, β, f_{GW} and narrower range of ρ_i/a, $\rho_{\theta i}/a$, a/R is covered by these tests.

Further testing of the model against a broader range of devices is underway, and possible extensions are being considered. Nonetheless, given initial success, it is useful to apply the model to ITER, to provide estimated pedestal values for use as inputs to other modeling and design activity. Using the Scenario 2 parameters, EPED1 predicts a pedestal height in ITER of $\beta_{N,ped}$=0.6–0.7, and a width Δ~0.04. Small variations around the Scenario 2 parameters allow optimization to values up to $\beta_{N,ped}$~0.8–0.9. At the ITER reference density of 10^{20} m^{-3}, and typical profile peakedness, yielding a pedestal density 7×10^{19} m^{-3}, a value of $\beta_{N,ped}$=0.65 corresponds to T_{ped}~4.6 keV.

6. Summary

The combination of high resolution diagnostics and an efficient suite of codes has allowed routine analysis of pedestal stability on many tokamaks. It is reasonably well established that Type I ELM onset is associated with the intermediate-n MHD stability boundary, while RMP ELM-free, high density Type III ELM, and EDA discharges operate below the ideal boundary. Models have been proposed for other types of small and no ELM discharges including Type II, grassy, and QH mode. Recent experiments, and analysis accounting for pedestal stability, suggest a pedestal width scaling similar to $\beta_{p,ped}^{1/2}$. Combining a simple width model with pedestal stability calculations, we have constructed a predictive model for the pedestal height and width (EPED1), which has proved accurate in an initial set of tests. Initial predictions for ITER have been made using this model. Work is ongoing to further test

and refine models, build theoretical understanding of the physics setting the pedestal width, and better understand small ELM regimes, including pellet induced ELMs.

Acknowledgments

References

[1] SNYDER, P.B. *et al.*, Phys. Plasmas **12**, 056115 (2005).
[2] CONNOR, J.W. *et al.*, Phys. Plasmas **5**, 2687 (1998).
[3] WILSON, H.R. *et al.*, Phys. Plasmas **9**, 1277 (2002).
[4] SNYDER, P.B. *et al.*, Phys. Plasmas **9**, 2037 (2002).
[5] MIKHAILOVSKII, A.B. *et al.*, Plasma Phys. Rep. **23**, 844 (1997).
[6] HUYSMANS, G.T.A., Plasma Phys. Control. Fusion **47**, B165 (2005).
[7] TOKUDA, S. and WATANABE, T., Phys. Plasmas **6**, 3012 (1999); AIBA, N. *et al.*, Comput. Phys. Commun. **175**, 269 (2006).
[8] AIBA, N. *et al.*, Plasma Fusion Res. **2**, 010 (2007).
[9] MEDVEDEV, S. Yu., *et al.*, Plasma Phys. Control. Fusion **48**, 927 (2006).
[10] KONZ, C., *et al.*, EPS Conf. on Plasma Physics (2008).
[11] TURNBULL, A.D., *et al.*, Plasma Phys. Control. Fusion **45**, 204 (2003).
[12] WILSON, H.R., *et al.*, Plasma Phys. Control. Fusion **48**, A71 (2006).
[13] SNYDER, P.B., *et al.*, Nucl. Fusion **47**, 961 (2007).
[14] SAARELMA, S., *et al.*, Plasma Phys. Control. Fusion **49**, 31 (2007).
[15] HUYSMANS, G.T.A., and CZARNY, O., Nucl. Fusion **47**, 659 (2007).
[16] BEURSKENS, M., *et al.*, Nucl. Fusion **48**, 095004 (2008).
[17] SAARELMA, S., *et al.*, submitted to Plasma Phys. Control. Fusion (2008).
[18] SNYDER, P.B., *et al.*, Plasma Phys. Control. Fusion **46**, A131 (2004).
[19] SAIBENE, G., et al., Nucl. Fusion **47**, 969 (2007).
[20] LEONARD, A.W., *et al.*, Phys. Plasmas **15** 056114 (2008).
[21] OYAMA, N. et al, Nucl. Fusion **45**, 871 (2005).
[22] LÖNNROTH, J-S, *et al.*, Plasma Phys. Control. Fusion **49**, 273 (2007).
[23] MOSSESSIAN, D.A., Phys. Plasmas **10**, 1720 (2003).
[24] MAGGI, C.F., *et al.*, Nucl. Fusion **47**, 535 (2007); MAGGI, C.F., *et al.*, EPS 2008.
[25] EVANS, T.E., *et al.*, Nature Phys. **2**, 419 (2006).
[26] LIANG, Y., *et al.*, Phys. Rev. Lett. **98**, 265004 (2007).
[27] LOARTE, A., *et al.*, Phys. Plasmas **11**, 2668 (2004).
[28] BURRELL, K.H., *et al.*, Fusion Energy 2008 (Proc 22 Int. Conf Geneva 2008, EX/8-4).
[29] ONJUN, T., *et al.*, Phys. Plasmas **9**, 5018 (2002).
[30] OSBORNE, T.H., *et al.*, J. Nucl. Mater. **266-269**, 131 (1999).
[31] URANO, H. , *et al.*, Nucl. Fusion **48**, 045008 (2008).
[32] GROEBNER, R.J. , *et al.*, Fusion Energy 2008 (Proc. 22nd Int. Conf. Geneva, EX/P3-5).
[33] SNYDER, P.B. , *et al.*, to be submitted to Phys. Plasmas 2008; TTF, Boulder USA (2008).
[34] DOYLE, E.J. , *et al.*, Fusion Energy 2008 (Proc 22nd Int. Conf. Geneva, EX/1-3).